https://ntrs.nasa.gov/search.jsp?R=20140004925 2019-08-29T14:34:38+00:00Z

NASA/TM—2013-216537

Improvements in High Speed, High Resolution Dynamic Digital Image Correlation for Experimental Evaluation of Composite Drive System Components

Lee W. Kohlman, Charles R. Ruggeri, Gary D. Roberts, and Robert F. Handschuh
Glenn Research Center, Cleveland, Ohio

July 2013

NASA STI Program . . . in Profile

Since its founding, NASA has been dedicated to the advancement of aeronautics and space science. The NASA Scientific and Technical Information (STI) program plays a key part in helping NASA maintain this important role.

The NASA STI Program operates under the auspices of the Agency Chief Information Officer. It collects, organizes, provides for archiving, and disseminates NASA's STI. The NASA STI program provides access to the NASA Aeronautics and Space Database and its public interface, the NASA Technical Reports Server, thus providing one of the largest collections of aeronautical and space science STI in the world. Results are published in both non-NASA channels and by NASA in the NASA STI Report Series, which includes the following report types:

- TECHNICAL PUBLICATION. Reports of completed research or a major significant phase of research that present the results of NASA programs and include extensive data or theoretical analysis. Includes compilations of significant scientific and technical data and information deemed to be of continuing reference value. NASA counterpart of peer-reviewed formal professional papers but has less stringent limitations on manuscript length and extent of graphic presentations.

- TECHNICAL MEMORANDUM. Scientific and technical findings that are preliminary or of specialized interest, e.g., quick release reports, working papers, and bibliographies that contain minimal annotation. Does not contain extensive analysis.

- CONTRACTOR REPORT. Scientific and technical findings by NASA-sponsored contractors and grantees.

- CONFERENCE PUBLICATION. Collected papers from scientific and technical conferences, symposia, seminars, or other meetings sponsored or cosponsored by NASA.

- SPECIAL PUBLICATION. Scientific, technical, or historical information from NASA programs, projects, and missions, often concerned with subjects having substantial public interest.

- TECHNICAL TRANSLATION. English-language translations of foreign scientific and technical material pertinent to NASA's mission.

Specialized services also include creating custom thesauri, building customized databases, organizing and publishing research results.

For more information about the NASA STI program, see the following:

- Access the NASA STI program home page at *http://www.sti.nasa.gov*

- E-mail your question to *help@sti.nasa.gov*

- Fax your question to the NASA STI Information Desk at 443–757–5803

- Phone the NASA STI Information Desk at 443–757–5802

- Write to:
  STI Information Desk
  NASA Center for AeroSpace Information
  7115 Standard Drive
  Hanover, MD 21076–1320

NASA/TM—2013-216537

Improvements in High Speed, High Resolution Dynamic Digital Image Correlation for Experimental Evaluation of Composite Drive System Components

Lee W. Kohlman, Charles R. Ruggeri, Gary D. Roberts, and Robert F. Handschuh
Glenn Research Center, Cleveland, Ohio

Prepared for the
69th Annual Forum and Technology Display (AHS Forum 69)
sponsored by the American Helicopter Society
Phoenix, Arizona, May 21–23, 2013

National Aeronautics and
Space Administration

Glenn Research Center
Cleveland, Ohio 44135

July 2013

Acknowledgments

Funding for this work has been provided by NASA's Rotary Wing Project. Assistance with the accelerometer data collection was provided by Kelsen LaBerge and Paula Dempsey at NASA Glenn Research Center. Ongoing analysis of the accelerometer data is being performed by Han DeSmidt of the University of Tennessee.

Trade names and trademarks are used in this report for identification only. Their usage does not constitute an official endorsement, either expressed or implied, by the National Aeronautics and Space Administration.

This work was sponsored by the Fundamental Aeronautics Program at the NASA Glenn Research Center.

Level of Review: This material has been technically reviewed by technical management.

Available from

NASA Center for Aerospace Information
7115 Standard Drive
Hanover, MD 21076–1320

National Technical Information Service
5301 Shawnee Road
Alexandria, VA 22312

Available electronically at http://www.sti.nasa.gov

Improvements in High Speed, High Resolution Dynamic Digital Image Correlation for Experimental Evaluation of Composite Drive System Components

Lee W. Kohlman, Charles R. Ruggeri, Gary D. Roberts, and Robert F. Handschuh
National Aeronautics and Space Administration
Glenn Research Center
Cleveland, Ohio 44135

Abstract

Composite materials have the potential to reduce the weight of rotating drive system components. However, these components are more complex to design and evaluate than static structural components in part because of limited ability to acquire deformation and failure initiation data during dynamic tests. Digital image correlation (DIC) methods have been developed to provide precise measurements of deformation and failure initiation for material test coupons and for structures under quasi-static loading. Attempts to use the same methods for rotating components (presented at the AHS International 68th Annual Forum in 2012) are limited by high speed camera resolution, image blur, and heating of the structure by high intensity lighting. Several improvements have been made to the system resulting in higher spatial resolution, decreased image noise, and elimination of heating effects. These improvements include the use of a high intensity synchronous microsecond pulsed LED lighting system, different lenses, and changes in camera configuration. With these improvements, deformation measurements can be made during rotating component tests with resolution comparable to that which can be achieved in static tests.

Introduction

A new high speed DIC measurement technique was used to measure the deformation near a damaged site for a composite tube rotating at 5000 rpm at torques up to 1130 Nm (10,000 in.-lb) and to examine the deformation of a diaphragm element of a flexible composite coupling also rotating at 5000 rpm at torques up to 1130 Nm (10,000 in.-lb). These results will be presented along with results of an initial attempt to detect damage in the rotating composite tube by processing of accelerometer data taken at the bearing mounts.

Previous testing presented by Kohlman (Ref. 1) showed that digital image correlation on high speed rotating components is primarily limited by lighting and exposure times. Tests performed using metal halide based continuous lighting was not sufficient to provide enough light without causing excessive heating of the test article and was not suitable to sustained operation. The result was longer camera shutter times which causes more image blur and higher noise levels. To get to the required illumination levels without excessive heating, an image synchronous pulsed LED illumination source was used. The LED based system is capable of very short pulse durations with fast rise and fall times and high repetition rates. Commercially available drivers capable of 2 μsec pulses were used, though shorter pulse drivers could be constructed for shorter exposure. The result was DIC results with noise levels comparable to stationary imaging.

These improvements will allow for more precise data to be collected on composite rotating structure with sufficient resolution to identify local damage and failure processes during operation. Rotation and torque tests were performed using a composite tube with varying levels of damage and with a composite flexible element. These tests were performed in the High Speed Helical Gear Test rig at NASA Glenn Research Center. More information on the test rig is provided by Handschuh (Refs. 2 to 4). Acceleration data was also collected at the bearing mounts to determine if the damage could be detected remotely.

A high resolution camera system is also being developed that uses a pair of 29 megapixel cameras and pulsed LED lighting to acquire higher resolution images and further improve the capability for damage detection in rotating composite structures.

Synchronous Pulsed Led Lighting

LED lighting can be used to produce extremely intense pulses of light with high repetition, fast rise and fall times, and short duration (Refs. 5 and 6). Most LEDs available today are typically limited to only a few watts. To achieve the high level of illumination required, many individual LEDs are needed. Because the LEDs are operated in a pulsed mode with a very low duty cycle, heat dissipation of the array is not a significant concern, however the individual LED experiences rapid heating and cooling and severe electrical stresses.

First Generation LED Array

A compact LED array, shown in Figure 1, was constructed to provide the high illumination required for the short duration exposures required by the high speed imaging. The array is composed of 90 Cree XM-L 4500 k white LEDs rated at 1.5 A maximum continuous current. The LEDs were individually fitted with 12 degree optics (typically specified for Cree XP-G LEDs) and a 45.7 cm (18 in.) focal length

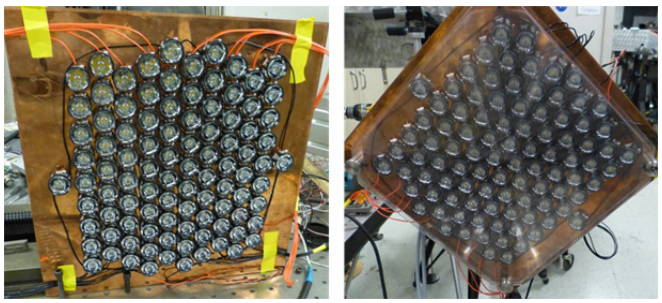

Figure 1.—High intensity pulsed LED light array.

Fresnel lens was used to focus the light into an area roughly 15.2 cm (6 in.) square. The LEDs are connected in series (9 LEDs per string) with 5 strings wired in parallel. Each set of 5 strings were connected to one channel of an Advanced Illumination Pulsar 320 LED driver that supplies 2 channels at 50 A per channel or 10 A per string (6.7 times the continuous rated LED current). The LEDs were operated with pulse duration of 2 μsec with an effective driving power of approximately 3000 W. Heating of the composite test article due to the lighting, as was previously experienced using 1200 W of metal halide lighting, was not a limitation because the short pulse duration and relatively low repetition rate (<1000 Hz) results in an average power of less than 6 W. Six additional LEDs are operated continuously to enable positioning of the array. The pulsed illumination appears very dim to the human eye because of the low duty cycle.

An image of the cameras, LED array (copper plate in front of the cameras), and composite tube installed in the test rig is shown in Figure 2. The high speed cameras are Phantom V10 cameras with a 4 megapixel black and white sensor. The triggering method is similar to the previously reported system (Ref. 1) except for the addition of the LED system and a variable timing delay between camera and LED trigger signals provided by the microcontroller. Before synchronous operation, the camera and LED triggers are operated at a user specified frequency to avoid timeout. A button on the microcontroller switches the microcontroller over to synchronous operation at the beginning of the test. An optical sensor is used to provide a pulse as reflective strips on the shaft pass by. One or multiple reflective strips can be used. The microcontroller counts the pulses from the optical sensor and triggers the cameras at the desired locations and rotation intervals. In this way, one location or the entire shaft can be imaged at any rotation interval. The separate trigger signals provided by the microcontroller allow for sub-microsecond compensation of the trigger latency difference between the cameras and LED driver.

Second Generation LED Array

After the first LED array was successfully tested, a second more compact array was designed. The new array will be 10.2 cm (4 in.) square and made from aluminum instead of copper. A rendering is shown in Figure 3. This array differs in several important ways from the first version. This array uses 14 LEDs wired in series to take better advantage of the driver's voltage capability. Two arrays will be wired in parallel to each channel of the driver so that up to 25 A (more than 16 times the rated continuous current) will be delivered to each LED instead of the previous 10 A. Also, each LED is mounted to a separate surface on the mounting plate that is angled such that all LEDs converge at a distance of 45.7 cm (18 in.). By angling each LED, the secondary Fresnel lens was eliminated, resulting in less scattering and absorption. The arrays will also be lighter and smaller making setup easier and allowing for lighting from multiple angles. Four panels will be driven by a single driver and supply almost 50 percent more light than the original array with 34 fewer LEDs.

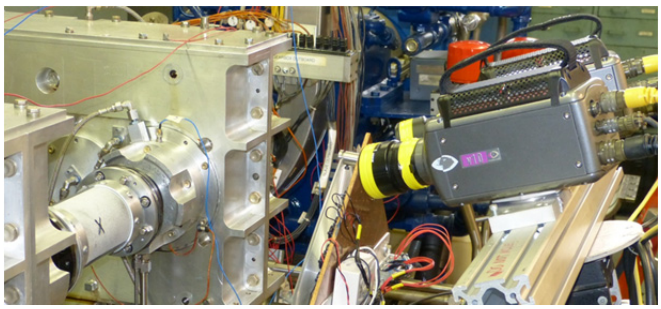

Figure 2.—Image of the cameras (right), LED array (middle), and shaft (left).

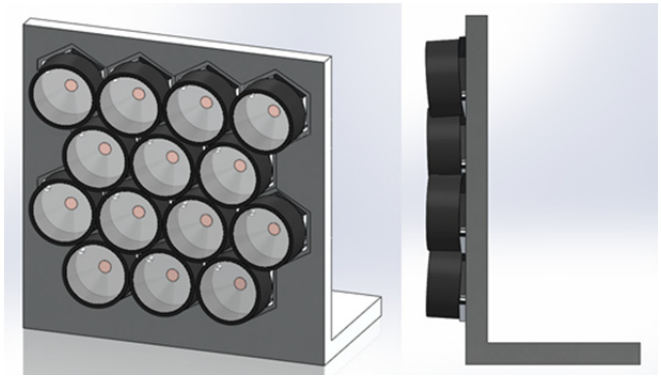

Figure 3.—Rendering of the second generation LED array.

Rotating Composite Structure

Failure of composite structure, particularly those with large fiber architecture, can often be attributed to initiation at local defects or damage sites. For example, the onset of a torsional buckling instability or material failure of a tube could be initiated by a local non-uniform deformation region near a defect or damage site in the tube. In previous quasi-static testing of flat coupons and tubes, localized high strain deformation and the onset of localized damage (e.g., splitting within fiber bundles and delamination between fiber tows) could be detected using full field DIC with appropriate camera resolution, lenses, and field of view. (Refs. 7 to 9). As

mentioned earlier in this paper, it is not currently possible to get the same spatial resolution in DIC measurements on rotating structures. This paper describes advancements that have been made to enable detection of local material deformation near a damage site in a rotating tube. Also described are further advancements that are in progress to enable measurement of damage such as splitting of fiber bundles and inter-tow delamination in a rotating structure at resolutions comparable to that achievable in current static tests.

Rotating Composite Tube Test

Preliminary testing of the high speed DIC method on a rotating composite tube was reported by Kohlman (Ref. 1) in 2012. A second shaft was constructed using the previously reported methods. The same quasi-isotropic triaxial braid construction was used.

Evaluation of the new pulsed LED system was performed on the new composite tube with 3 levels of damage (undamaged, an offset 6.35 mm (1/4 in.) diameter thru-drilled hole, and an "X" notch cut through the 6.35 mm (1/4 in.) hole with a cut off wheel). The "X" notch damaged tube is shown installed in Figure 4. Tests were performed at various speeds and torques to determine DIC noise levels and minimum strain and displacement resolution and for collection of accelerometer data. The accelerometers are visible on the bearing mounts at the ends of the blue wires in Figure 4. Analysis of the accelerometer data is ongoing.

Data were collected under the following conditions for the composite tube in all three damage states:

1. Speed ramp to 5000 rpm immediately followed by a torque ramp to 1130 Nm (10,000 in.-lb) or roughly 560 kW (750 hp)
2. Speed step increase (1000, 2000, 3000, 4000, and 5000 rpm) with a 113 Nm (1000 in.-lb) torque applied to prevent chatter
3. Torque step increases at 113, 282, 565, 847, and 1130 Nm (1000, 2500, 5000, 7500, and 10,000 in.-lb) at 5000 rpm
4. Speed step decrease (5000, 4000, 3000 rpm) at full torque (1130 Nm or 10,000 in.-lb)

Figure 5 (top) is a plot of the standard deviation of major strain at different operating speeds with 113 Nm (1000 in.-lb) torque. The values of major strain were taken from the location shown in the major strain map (Fig. 5, bottom). Ten stages were used at each operating speed to calculate the standard deviation. There is little dependence of standard deviation on operating speed and all values are very low, less than 0.03 percent at this location. Variation is expected to increase near the edges of the measurement region because of a greater out-of-plane component and the images become out-of-focus. This also results in the elliptic measurement region visible in the major strain map on the bottom in Figure 5. Previous testing using metal halide lighting showed a significant increase in variation with speed and required the

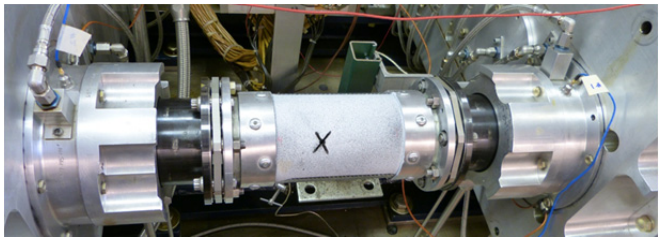

Figure 4.—Composite tube in machine with the most severe damage "X" notch.

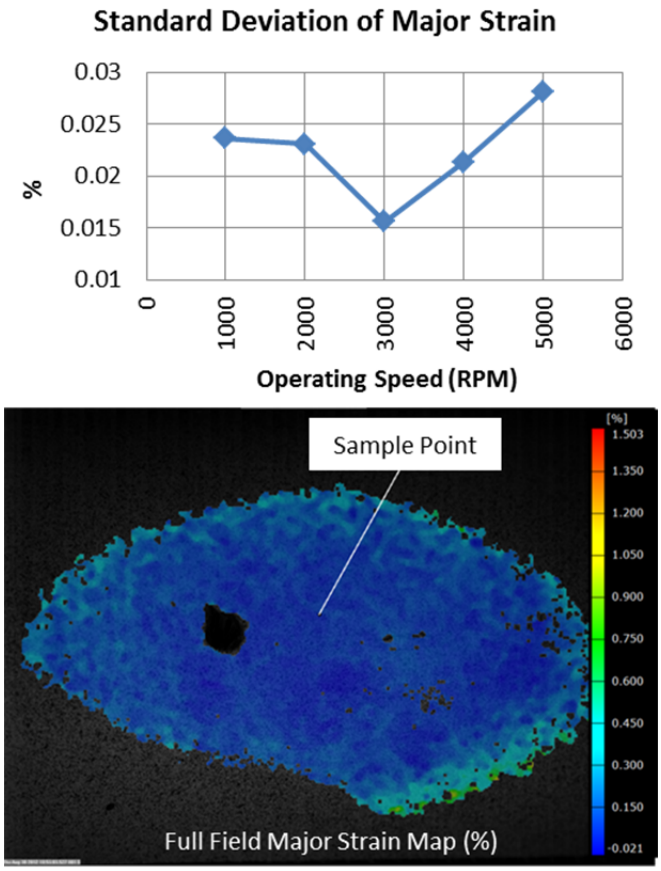

Figure 5.—Plot of the standard deviation of major strain at different rotational speeds (top) and an example major strain map showing the point used for the standard deviation measurement (bottom).

limit on a parameter in the DIC software known as intersection deviation to be raised to 1.5 pixels to successfully process the DIC project. Data acquired with the new system was successfully processed at the default value of 0.3 pixels. The data in Figure 5 were collected on the damaged composite tube with the 6.35 mm (1/4 in.) diameter hole, visible in the image on the bottom.

Figure 6 is an example of the resolved radial displacement (top) and shear strain (bottom) observed near the "X" notch in the composite tube. Due to the relatively thick tube wall and torque limited to 1130 Nm (10,000 in.-lb), very little deformation was observed in the undamaged test. Previous

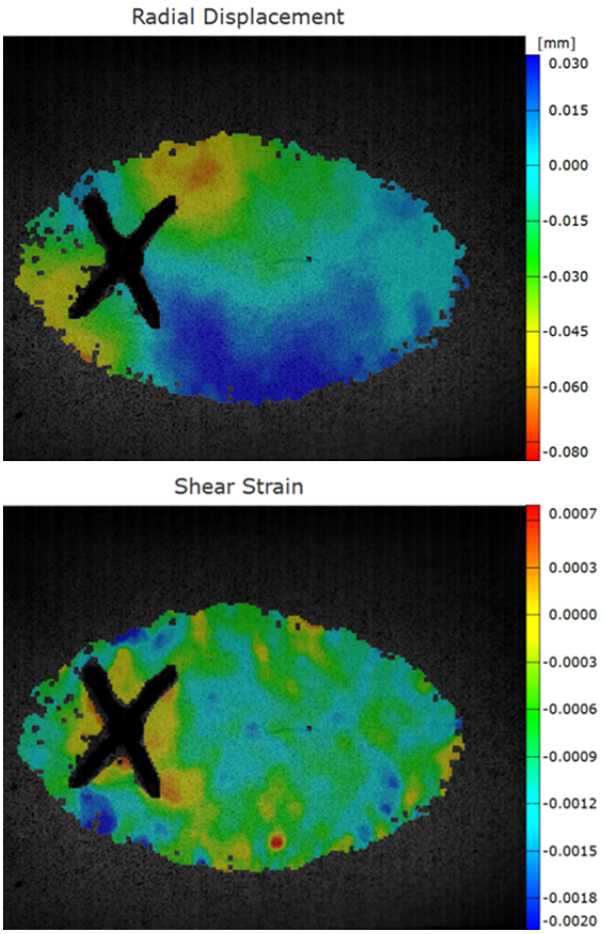

Figure 6.—An example of torque induced radial displacement (top) and shear strain (bottom) around the "X" notch in the composite tube at 5000 rpm and 1130 Nm (10,000 in.-lb).

tests on an impact damaged composite tube showed similar patterns but were very difficult to identify except at the highest loading. The failure torque of the undamaged composite tube is expected to exceed 9040 Nm (80,000 in.-lb). The tube was not tested to failure in a static test, however a similar tube with a known mold line defect was tested and failed at 6200 Nm (55,000 in.-lb) with failure initiating at the defect site.

Composite Flexible Element

Flexible shaft couplings add a significant amount of weight to rotorcraft drive systems. One possible concept to reduce the weight of these components is to construct a flexible element which is integral to the shaft. This eliminates the need for additional fasteners and flanges, however the durability and fatigue characteristics of such a structure is an area warranting more detailed investigation. High speed DIC on these structures could provide data needed for model development and assist with damage detection and deformation mode

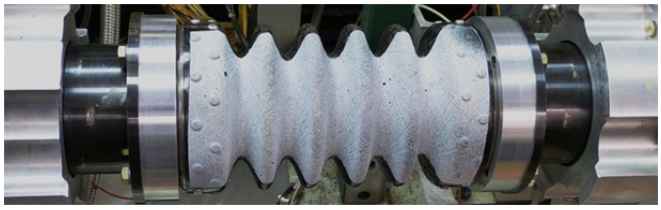

Figure 7.—Filament wound flexible composite element mounted in the test rig.

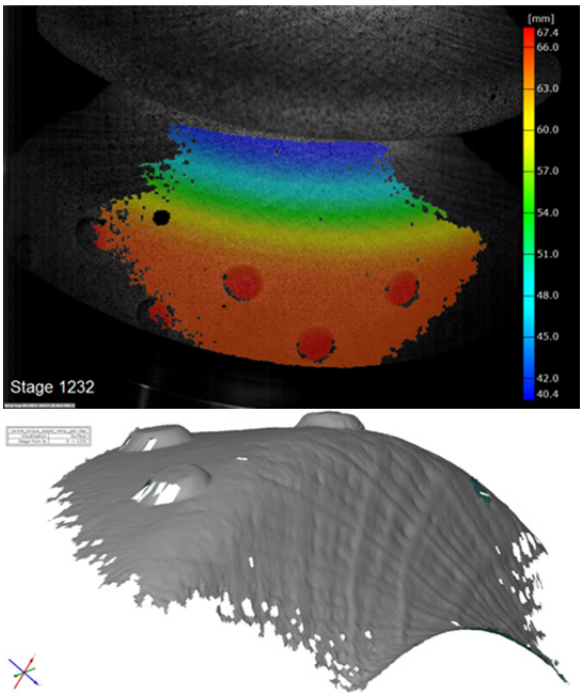

Figure 8.—Close-up DIC at 5000 rpm on a filament wound composite flex element showing local radius measurement (top), and resolved local surface texture (bottom).

characterization during operation. In order to evaluate the high speed DIC methods on a coupling with complex shape, filament wound flexible elements were acquired from Lawrie Technology, Inc. These flexible elements have a more complex geometry and smaller tow size than the previously tested composite tubes. Tests that were performed included some of the various speed and torque conditions used in the damaged tube tests. The mounted test article is shown in Figure 7.

Figure 8 shows examples of the resolved features in a small section near one end of the test element. Again, the improved lighting reduces measurement noise and allows for the use of a smaller field of view on the test article while operating at 5000 rpm. 100 mm lenses were used for this test and the cameras were mounted such that the intersection of the focal planes was parallel to the rotation axis (the camera assembly was tilted 90° compared to what is shown in Fig. 2).

At the load limit of 1130 Nm (10,000 in.-lb), very little deformation was observed.

High Resolution DIC

Higher resolution images allow for more detailed investigation of composite damage and failure under load (Refs. 7 to 9). A custom camera system is being built to acquire images for DIC using a pair of 29 megapixel machine vision cameras. The GX6600 camera from Allied Vision was selected for this system. This camera uses the Kodak Truesense KAI-29050 sensor with a resolution of 6576 by 4384 pixels.

This camera is capable of a minimum shutter of 30 μsec but, with the pulsed illumination method, it may be possible to achieve effective shutter times of 2 μsec with the current LED drivers. Figure 9 is a sketch of the new camera system operational layout. A position sensor provides a signal to the Camera and LED Controller which then triggers the LED drivers and Cameras. Images from the Cameras are then saved to the Acquisition Computer using dual gigabit Ethernet (GigE) lines with Link Aggregation from each camera. The Acquisition Computer uses a quad GigE PCI Express card and a striped RAID 0 hard drive array to maintain the maximum data transfer rates. The Camera and LED Controller consists of a mini-ITX computer case with a Raspberry Pi microcontroller and interfacing circuit installed within. Power for the cameras and Raspberry Pi is supplied by the built-in ATX power supply. The Raspberry Pi operates with a Debian Linux operating system and can be controlled wirelessly (USB WIFI dongle) via a Secure Shell (SSH). The Acquisition Computer operates with an Ubuntu Linux operating system and can also be interfaced using SSH. Images can be transferred from the Acquisition Computer to another computer using FTP or any other desired file transfer protocol using the onboard (5th) GigE adapter.

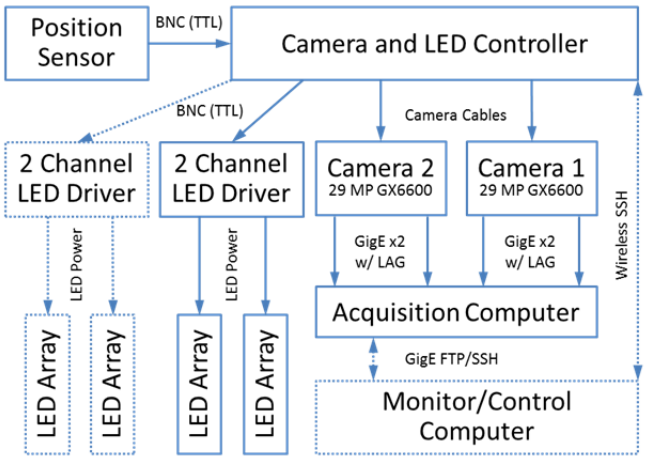

Figure 9.—Mode of operation schematic.

A simple 2D demonstration was performed with the 29 megapixel cameras to show that the larger images can be used with existing DIC software and to document the possible increase in data resolution. The demonstration used a single camera and a 100 mm lens with a working distance of roughly 45.7 cm (18 in.). The camera was then calibrated using the 2D DIC procedure. The field of view was roughly 8 by 10 cm (3.1 by 3.9 in.). Figure 10 (top) shows a previously tested braided composite coupon with the same architecture as the composite tube discussed earlier. A stochastic pattern was applied using a fine spray paint mist. The scale bar is approximate. The combination of increased resolution and narrow optics resulted in spatial resolution greater than 55 pixels/mm (1400 pixels/inch). The DIC facet and step size were set to 11 and 7 pixels, respectively. This generated a data resolution of 8 data points/mm (200 data point/inch). The bottom of Figure 10 shows a close up of the image with the data point grid (7 pixel spacing) overlaid. A single tow 3.5 mm (0.14 in.) wide is visible. The 29 megapixel DIC is capable of resolving much smaller features while increasing the overall field of view.

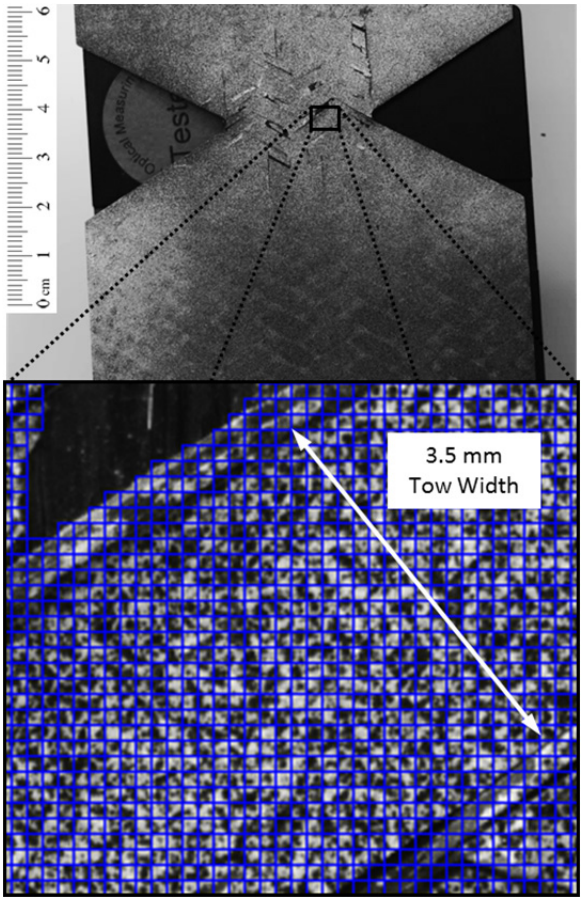

Figure 10.—29 megapixel image (top) and data point grid (bottom).

Conclusions

The high intensity synchronous pulsed LED illumination method was successful in reducing the noise during image capture on rotating composite components for digital image correlation measurement. The effects of blur were minimized and noise levels comparable to static operation were observed. Also, heating of the component was eliminated by replacing the high intensity metal halide lights used previously with more intense, but low duty cycle LED illumination. Development of the high resolution DIC system is underway and preliminary tests indicate that no difficulties with the commercially available DIC software are expected when processing the larger images. The achievable field of view and spatial resolution will allow more detailed investigation of the local damage and failure mechanisms of the composite architecture. Synchronous pulsed illumination is expected to produce effective shutter times of 2 μsec with the 29 megapixel cameras (minimum shutter time of 30 μsec), but this has not yet been tested. A higher torsion load limit is required to produce damage and/or failure in the components tested to better demonstrate the capability of detecting local damage during rotational operation.

References

1. Kohlman, L.W., Ruggeri, C.R., Martin, R.E., Roberts, G.D., Handschuh, R.F., and Roth, D.J., "Full-field Deformation Measurement Techniques for a Rotating Composite Shaft," American Helicopter Society 68th Annual Forum Proceedings, Fort Worth, TX, May 2012.
2. Handschuh, R. and Kilmain, C., "Experimental Study of the Influence of Speed and Load on Thermal Behavior of High-Speed Helical Gear Trains," NASA TM-2005-213632, July 2005.
3. Handschuh, R. and Kilmain, C., "Operational Influence on Thermal Behavior of High-Speed Helical Gear Trains," NASA TM-2006-214344, November, 2006.
4. Handschuh, R., Kilmain, C., and Ehinger, R., "Operational Condition and Superfinishing Effect on High-Speed Helical Gearing System Performance," NASA TM-214696, June 2007.
5. Aikio, M., Lindström, H., Juntunen, E., Kataja, K., and Keränen, H., "Pulsed LED Illumination for High Speed Imaging," *Key Engineering Materials*, Vols. 364-366, 2008, pp. 827-831. doi:10.4028/www.scientific.net/KEM.364-366.827
6. Willert, C., Stasicki, B., Klinner, J., and Moessner, S. "Pulsed Operation of High-Power Light Emitting Diodes for Imaging Flow Velocimetry," *Measurement Science and Technology*, Vol. 21, June 2010, pp. 1-11. doi:10.1088/0957-0233/21/7/075402
7. Kohlman, L.W., "Evaluation of Test Methods for Triaxial Braid Composites and the Development of a Large Multiaxial Test Frame for Validation Using Braided Tube Specimens," Ph.D. Dissertation, The University of Akron, Akron, Ohio, 2012.
8. Kohlman, L.W., Bail, J.L., Roberts, G.D., Salem, J.A., Martin, R.E., and Binienda, W.K., "A notched coupon approach for tensile testing of braided composites," *Composites: Part A*, Vol. 43, Issue 10, October 2012, pp. 1680-1688. doi: 10.1016/j.compositesa.2011.12.013
9. Littell, J.D., "The Experimental and Analytical Characterization of the Macromechanical Response of Triaxial Braided Composite," Ph.D. Dissertation, The University of Akron, Akron, Ohio, 2008.